Exsolution and alteration microtextures in alkali feldspar phenocrysts from the Shap granite

MARTIN R. LEE, KIM A. WALDRON* AND IAN PARSONS

Department of Geology and Geophysics, The University of Edinburgh, West Mains Road, Edinburgh, EH9 3JW, Scotland

Abstract

Alkali feldspar phenocrysts (bulk composition $Or_{75.0}Ab_{24.6}An_{0.4}$) in the subsolvus Shap granite comprise a fine-scale mixture of subregular pristine crypto- and micro-perthites with altered, micropore-rich feldspar with irregular microstructures. The regular perthites are strain-controlled intergrowths of Albite and/or Pericline-twinned albite exsolution lamellae within tweed orthoclase. The microperthites formed at $\leqslant 590°C$ by heterogeneous nucleation of thin albite films which coarsened to > 1 μm length. Cryptoperthites developed at < 400°C by homogeneous nucleation of sub-μm long platelets between films. Platelets are coherent, but the coarser microperthite lamellae are semi-coherent, with pairs of misfit dislocations sub-regularly spaced along the albite–orthoclase interface. As much as 30% of any one feldspar crystal is turbid, a result of the formation of numerous μm to sub-μm sized micropores during deuteric alteration. In some areas, deuteric fluids gained access to the interior of feldspar crystals by exploiting semi-coherent film lamellae. Albite was selectively dissolved and micropore-rich irregular microcline was reprecipitated in its place. In other parts of the feldspars deuteric recrystallization completely cross-cuts the pristine microtextures and patch perthites have formed. These are coarse, incoherent to semi-coherent intergrowths of irregular microcline (replacing tweed orthoclase) and Albite-twinned albite. The deuteric reactions occurred at < 400°C; the main driving force for dissolution and reprecipitation was decrease in the elastic strain energy at the coherent interfaces of crypto- and micro-perthite lamellae, and the recrystallization of tweed orthoclase to irregular microcline.

KEYWORDS: alkali feldspar, argon systematics, deuteric alteration, dislocations, electron microscopy, etching, exsolution, granite, orthoclase, microcline, perthite.

Introduction

THE striking, large pink alkali feldspar phenocrysts from the granite exposed and quarried near Shap in Cumbria, north-west England, frequently figure in elementary teaching collections and are thus well known to generations of British geologists. However, despite their familiarity, no detailed microtextural work has been published on these crystals. We here describe in detail their microstructure, in particular their exsolution microtextures and the relationships between turbidity, alteration and pristine microtextures. The Shap phenocrysts have many features which we know from our work on other intrusions are representative of potassium feldspars from many sub-solvus granitic rocks. We stress the importance of a new method for the investigation of feldspar microstructures, recently described by Waldron *et al.* (1994), which involves the imaging by scanning electron microscopy (SEM) of cleavage fragments etched with hydrofluoric acid. This method bridges the critical gap in scales between optical/back-scattered electron (BSE) imaging and transmission electron microscopy (TEM). Moreover, by using this technique, the relationship between defects such as

*Present address: Department of Geology, Colgate University, Hamilton, NY 13346, USA

Mineralogical Magazine, March 1995, Vol. 59, pp. 63–78

dislocations at lamella interfaces and exsolution microstructures can be studied in unprecedented detail.

Despite the conspicuous appearance and abundance of Or-rich alkali feldspar phenocrysts in subsolvus granitic igneous rocks, the microstructures of these perthitic crystals have received little attention, perhaps because turbidity (and the complex, rather chaotic microtextural changes which accompany its development) often obscures pristine exsolution microtextures. Recent TEM work on perthites has shown a complicated interrelationship between turbidity and exsolution microtextures (Worden *et al.*, 1990; Guthrie and Veblen, 1991; Fitz Gerald and Harrison, 1993). The little previous TEM work on Or-rich crypto- and micro-perthites has shown that the regular microstructures are coherent or periodically semicoherent (Aberdam, 1965; Gandais *et al.*, 1974; Brown and Parsons, 1984). As we show below, the extremely varied microstructures may be used to obtain information on the thermal history of the crystals, and on fluid–feldspar interactions during cooling. The textures are also important in the field of $^{40}Ar/^{39}Ar$ 'thermochronometry' (Zeitler and Fitz Gerald, 1986; Fitz Gerald and Harrison, 1993).

Experimental technique

The Shap granite alkali feldspar phenocrysts have been investigated using light microscopy, SEM, electron probe microanalysis (EPMA) and TEM. BSE images were obtained from randomly-oriented feldspar crystals in polished thin sections and both polished and unpolished cleavage fragments using a Cambridge Instruments S250 SEM. Feldspar cleavage fragments of known crystallographic orientation were also gently etched in HF vapour, following the technique of Waldron *et al.* (1994), gold coated and then imaged in the SEM using secondary electrons (SE). This technique allows K to be distinguished from Na feldspar by differences in their etching rates. The resolution of these SE images (< 50 nm) is significantly greater than that of BSE images (~250 nm). EPMA was carried out using a Cameca Camebax electron microprobe operated at 15 kV and with a beam current of 10 nA. The electron beam was rastered in order to minimise Na loss.

Feldspar crystals oriented close to (001) were extracted from polished thin sections, argon ion beam thinned until electron-transparent and examined using a Philips CM12 TEM operated at 120 kV. All images and diffraction patterns were acquired with the electron beam near to the [001] or [102] zone axes. High-resolution and lattice images were obtained with the same instrument, using a Gatan image intensifier system for focusing.

Geological background

The Shap granite crops out over an area of ~5.5 km^2 to the south of Shap in Cumbria, north-west England. It is an early Devonian (Rb–Sr age of 394±3 Ma; Wadge *et al.*, 1978) composite biotite-granite intrusion which is quarried extensively as an ornamental stone. The Shap granite is part of a Lower Palaeozoic batholith which underlies much of the Lake District of north-west England (Bott, 1974; Lee, 1986). It forms a steep-sided, cone-shaped igneous body (Locke and Brown, 1978) and was intruded into the Ordovician Borrowdale Volcanic Series during a stress-relief episode late in the Caledonian orogeny (Soper and Kneller, 1990). The granite has experienced Ba-Bi-Cu-F-Mo-Zn mineralization which is widespread, although limited in extent (Grantham, 1928). Aspects of its petrology have been described by Nicholson (1868), Aveline *et al.* (1888), Harker and Marr (1891), Grantham (1928) and Caunt (1986). Contact metamorphism and fissure-related metasomatic alteration of the country rocks have been investigated by Harker and Marr (1893) and Firman (1957), respectively.

Description

Light microscopy

In hand specimen, the Shap granite contains distinctive euhedral pink alkali feldspar phenocrysts 10–50 mm long within a matrix of <2 mm sized crystals of pink alkali feldspar, plagioclase, quartz and biotite. Grantham (1928) also recorded apatite, epidote, monazite and rutile as accessories. Plagioclase lies in the oligoclase–andesine compositional range (Grantham, 1928; Caunt, 1986) and all crystals have been partially altered to sericite, but no sericitic alteration was detected within the alkali feldspars. Poikilitically enclosed within the alkali feldspar phenocrysts are sub-mm sized inclusions of discrete, non-perthitic plagioclase, quartz (often in granophyric intergrowth), biotite and titanite. All of the plagioclase inclusions have again been partially altered to sericite.

Each alkali feldspar crystal has both pristine and turbid areas. The pristine feldspar is predominantly a microperthite with numerous narrow, straight exsolution lamellae. Individual lamellae can be tens of μm in length and are ≤5 μm apart (Fig. 1). Within the microperthite occur μm-sized areas of pristine feldspar which apparently contain no exsolution lamellae. The proportion of turbid feldspar in any one crystal is highly variable, but averages ~10–30%. Turbid areas have a brownish colour in plane polarized light and their distribution within any one crystal may be in part controlled by the lamellar

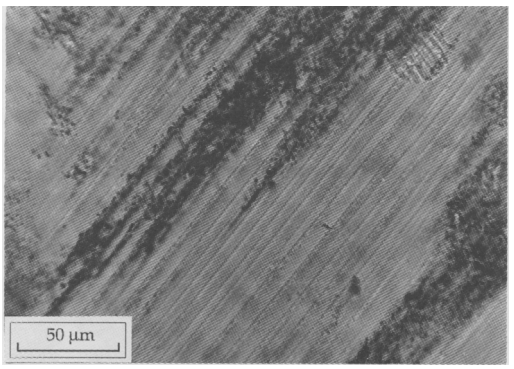

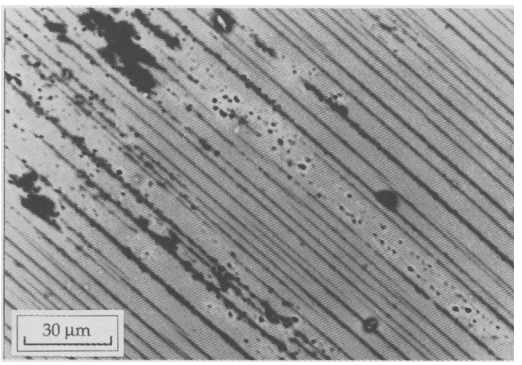

FIGS. 1 and 2. Fig. 1 (*left*). Plane light photomicrograph of an alkali feldspar phenocryst. Approximately 70% of the crystal contains pristine exsolution lamellae and the remainder is turbid. This turbidity is due to the presence of numerous fluid inclusions which can just be resolved at this magnification. Note that the turbidity is largely concentrated along zones which are parallel to the exsolution lamellae. Fig. 2 (*right*). BSE image (using SEM) of the phenocryst in Fig. 1. In some areas (just right of centre), exsolution lamellae have been completely removed, their place being taken by trains of micropores. In other areas (lower left), exsolution lamellae have been thickened, but these areas are again associated with micropores. More irregular patch perthites can also be seen (top left) in which albite-rich areas cross-cut the exsolution microtextures. The turbidity seen in light microscope images correlates closely with the density of these micropores.

microtexture (Fig. 1). Pristine microtextures are also cross-cut by anastomosing 100–150 μm wide veins of turbid alkali feldspar lacking lamellar exsolution features. The feldspar in these veins has a slightly different extinction position to that of the pristine areas and is often Albite-twinned. Small alkali feldspar crystals in the matrix of the Shap granite are zoned, with non-perthitic K-rich rims and perthitic cores.

Analyses of pristine and turbid alkali feldspars by EPMA using a rastered beam gave similar overall bulk compositions of $Or_{75.1}Ab_{24.5}An_{0.4}$ and $Or_{74.8}Ab_{24.8}An_{0.4}$ respectively. Individual analyses in turbid areas were, however, more variable that those of pristine feldspar, ranging from $Or_{68.5}Ab_{31.1}An_{0.4}$ to $Or_{82.6}Ab_{16.9}An_{0.5}$, presumably because of heterogeneity at a scale greater than the size of the rastered beam. The narrow zones of turbidity which run parallel to exsolution lamellae (Fig. 1) tend to be significantly more K-rich than the turbid areas which cross-cut the lamellae.

Backscattered electron microscopy

BSE images show that the pristine microperthites comprise long narrow Na-rich exsolution lamellae within a K-rich host (Fig. 2). Within these microperthites are 100–200 μm sized patches of pristine cryptoperthite in which the constituent exsolution lamellae are too small to be individually resolved. There is no systematic pattern in the spatial distribution of these cryptoperthitic patches within any one crystal.

The distribution of turbidity determined by light microscopy corresponds very closely to areas of altered feldspar which contain numerous micropores, < 250 nm to ~2 μm in size. In BSE images, these micropores have rounded outlines (Fig. 2), but SE images of the same areas show that their true shape is more angular. Part of the alteration has been selective to Na-rich lamellae. Some lamellae have been 'thickened' by irregular to euhedral outgrowths of Na feldspar, up to 3 μm in size, along some or all of their length (Fig. 2). Other lamellae have been partially or completely dissolved and their place has been taken by parallel 'trains' of micropores, adjacent trains having comparable spacings to those of pristine microperthite lamellae (Fig. 2). As these micropores have been formed by the removal of Na exsolution lamellae, the net result is to produce very K-rich areas (Fig. 2). The K feldspar between micropore trains appears to be micropore-free at the resolution of BSE images.

In addition to lamella-specific alteration, pristine microperthites and also occasionally the cryptoperthite patches are cross-cut by narrow (~20–50 μm wide) micropore-rich veins and larger, less regular patch perthites. The cross-cutting micropore-rich veins are again K-rich from the selective removal of Na feldspar. Patch perthites can cover areas hundreds of μm^2 in size and comprise irregular intergrowths of micropore-rich Na- and K-rich

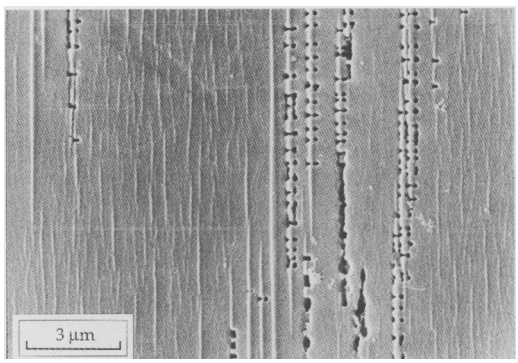

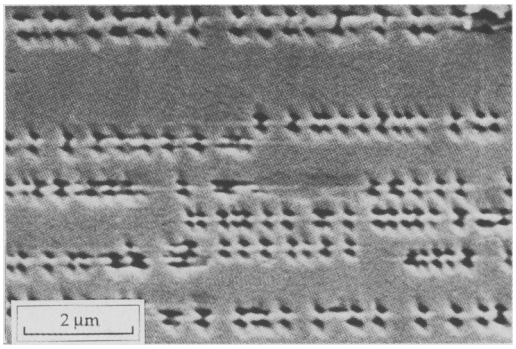

FIGS. 3 and 4. Fig. 3 (*left*). SE image of a HF-etched (001) cleavage fragment. Lamellae greater than ~100 nm in width are decorated by pairs of etch pits. Narrower lamellae and wedge-shaped ends of the wider lamellae have few or no etch pits. The platelet-rich area (left) is completely free of etch pits. To the right of centre, parts of some lamellae are absent. These parts correspond to the micropore-rich lamellae in Fig. 2. Fig. 4 (*right*). SE image of a HF-etched (010) cleavage fragment. Pairs of nm-sized etch pits with a distinctive two-fold symmetry straddle the exsolution lamellae. Note that where exsolution lamellae thin towards their wedge-shaped ends, etch pits die out and exsolution lamellae can no longer be distinguished.

feldspar (Fig. 2). Again, some areas have had wholesale Na removal and so are K-rich, whereas others are near-pure Na feldspar following the removal of K-feldspar.

Cleavage fragments etched with hydrofluoric acid

The HF etching technique allows investigation of perthite textures on scales of tens of μm to nm (Waldron *et al.*, 1994). Differences in the rates of etching of Na and K feldspar result in Na-rich areas standing out in relief. Na-rich exsolution lamellae are much more clearly defined on the (001) than (010) cleavage surfaces (Figs. 3 and 4) which indicates that the degree of difference in etching rates between Na and K feldspar is dependent upon crystallographic orientation. Because of these differences in etching rates, our work has concentrated on the (001) cleavage surface. Aberdam (1965) pioneered an etching technique to study dislocations in alkali feldspars. However, he had to use a TEM to image carbon replicas of the etched surfaces, and, because of these practical difficulties, his method was largely forgotten.

Pristine microtextures. Pristine Na-rich lamellae can be subdivided into platelets and films; platelets are less than ~1 μm long by ~75 nm wide and films are greater than ~1 μm long by ~75 nm wide. The separation of individual platelets ranges from ~100 to 250 nm, whereas films are 0 μm (in contact) to ~3.5 μm apart (mean ~1.0–1.5 μm). Although the platelets are most numerous in discrete cryptoperthitic patches, they also occur in small groups between films when the latter are >2 μm apart (Fig. 3). Images of the interface between the (001) and (010) cleavage surfaces show that the coarser film lamellae have an 'aeroplane wing' morphology, being much longer on the (010) than (001) cleavages (Waldron *et al.*, 1994). On both cleavage surfaces, all pristine lamellae have length/width ratios of >30 and taper to wedge-shaped ends (Figs. 3 and 4).

The most distinctive feature of the film lamellae where they intersect the etched surface is the presence of pairs of etch pits straddling them. The etch pits are sub-circular and ~100–125 nm in diameter on (001) and of similar size on the (010) cleavage surface but with distinct two-fold symmetry (Figs. 3 and 4). The spacing of etch pits along any one lamella is highly variable with standard deviations typically being ±50% of the mean spacing (Fig. 5). However, there is some correlation between mean etch pit spacing on (001) and lamella thickness. Those lamellae less than ~75 nm in maximum width have no etch pits or a few isolated ones (Fig. 3). Thicker lamellae (~100–400 nm in width) have numerous pairs of etch pits (Figs. 3 and 4) and mean etch pit spacing increases with lamella width (Fig. 5). Owing to the very large error bars about mean etch pit spacing for any one lamella (Fig. 5), this correlation is statistically poor. The Murchison plane ($\bar{6}01$) is the plane of exsolution in Or-rich alkali feldspars (and linear mesoperthites) and is the direction along which they can sometimes cleave. SE images of the Murchison plane following HF acid treatment show a regular network of grooves on the surface of K feldspar which is in direct contact with the lamellae (Fig. 6). One set of grooves is normal to (001) and the other normal to (010).

Alteration microtextures. Lamella-specific alteration has only affected the coarse film lamellae. These

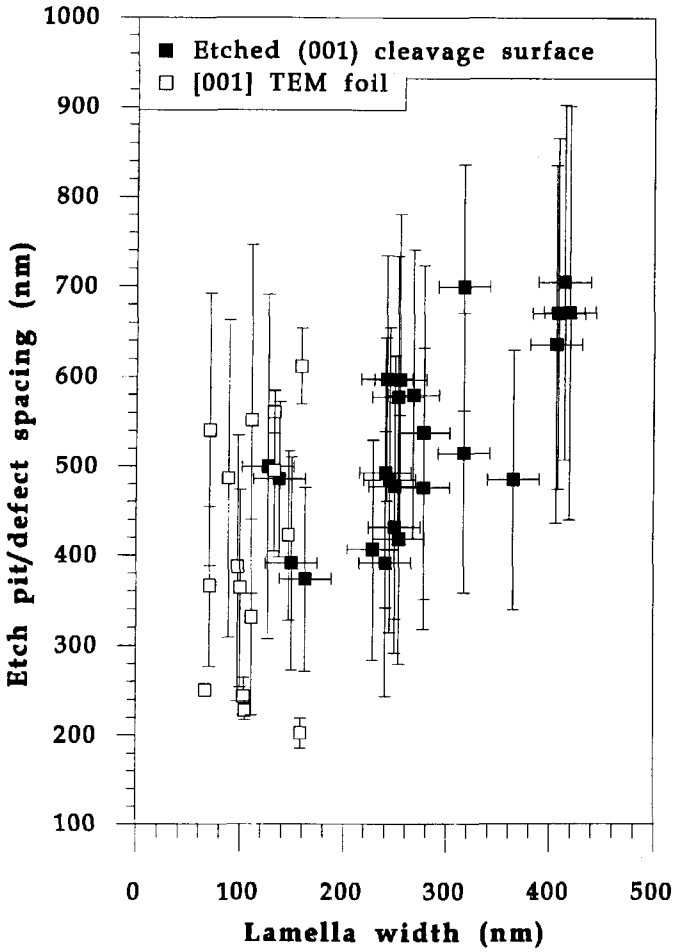

FIG. 5. Graph showing the correlation between the width of exsolution lamellae and the spacing of etch pits and defects (seen in TEM foils) along them. Vertical error bars represent the standard deviation of the spacing of etch pits/defects along each lamella. The number of spacing measurements for HF-etched samples was > 20, but only 3–6 for TEM foils. Horizontal error bars represent width measurement uncertainty (±25 nm on SE images).

thickened and micropore-rich lamellae have an overall morphology similar to the pristine film lamellae in tapering to wedge-shaped ends and having the vestiges of pairs of etch pits straddling them (Fig. 3). Alteration may affect entire lamellae or just parts of them. These altered lamellae have a strong tendency to occur together in discrete groups with surrounding films and platelets being completely unaffected (Fig. 3). Na feldspar that comprises thickened lamellae has numerous small micropores and an uneven etched surface, indicating the presence of subcrystals. The interface between outgrowths on thickened lamellae and the K-feldspar host may be uneven or more regular, delineated by {110} terminations. Despite complete removal of some film lamellae by alteration, leaving trains of coalesced micropores, the surrounding K-feldspar nearly always remains pristine (Fig. 3).

Patch perthites cross-cut microperthites and cryptoperthite patches alike. The etched surface of patch perthites is again uneven and pitted with numerous sub-μm sized micropores, some of which delineate μm-sized subcrystals (Fig. 7). The interface between patch perthites and surrounding K-feldspar may be uneven or regular along {110} terminations (Fig. 7).

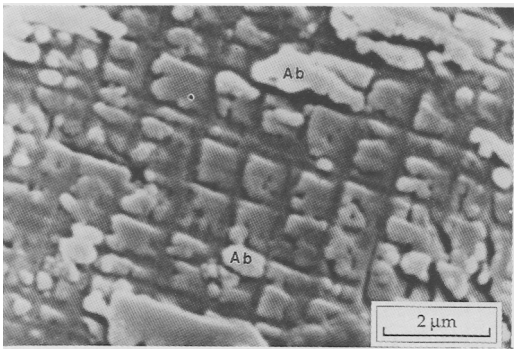

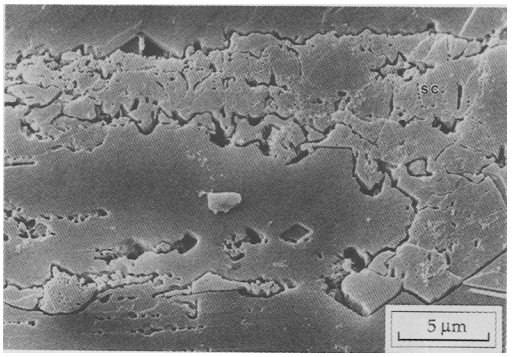

FIGS. 6 and 7. Fig. 6 (*left*). SE image of a HF etched Murchison plane. This image shows K-feldspar where an overlying exsolution lamella has been largely removed during sample preparation, leaving some albite remnants (Ab). On the surface of the K-feldspar is a grid of intersecting grooves, one set normal to (001), trending WNW–ESE on the micrograph, the other normal to (010), trending NNE–SSW. These grooves represent the etched expression, on the Murchison plane, of the sets of etch pits seen in Figs 3 and 4. Fig. 7 (*right*). SE image of a HF etched (001) cleavage fragment. The regular exsolution microtexture has been altered to an area of secondary K and Na-feldspar within featureless unaltered K-feldspar. A few etched film lamellae occur near the bottom left. Note the abundance of {110} Adularia habit terminations at the interface between altered and unaltered feldspar. The surface of this secondary feldspar has many small pits, some of which possibly delineate subcrystals (sc).

Transmission electron microscopy

Pristine microtextures. TEM images and selected area electron diffraction (SAED) patterns of pristine feldspar show albite exsolution lamellae oriented parallel to b^* in orthoclase. The orthoclase has diffuse tweed modulations ~6–13 nm in width and at the TEM scale is weakly triclinic (γ^* ~90.5°). The majority of film albite lamellae are in part Albite-twinned and in part untwinned (Figs. 8, 9 and 15). SAED patterns of such lamellae show groups of three reflections in which Albite twin spots straddle a central reflection from what appears in this orientation to be untwinned albite. The interface between the Albite-twinned albite lamellae and tweed orthoclase is finely corrugated, whereas the interface between untwinned albite and orthoclase is planar (Fig. 9).

Platelets can be as small as 30 nm long by 5 nm wide and only occur where film lamellae are > 200 nm apart (Fig. 10). The platelets may be untwinned (especially the smallest ones) or Albite-twinned.

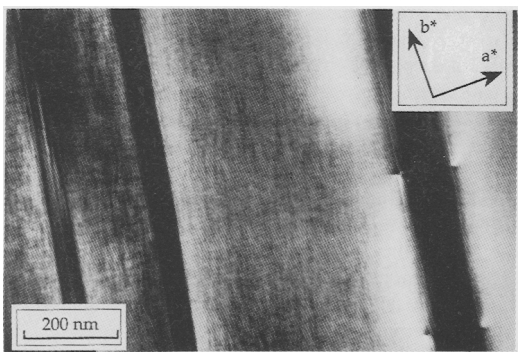

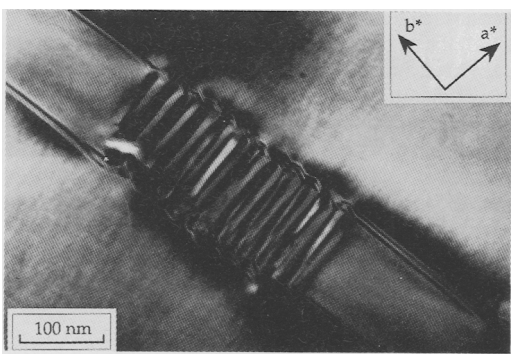

FIGS. 8 and 9. Fig. 8 (*left*). Bright-field TEM image of apparently untwinned, pristine albite exsolution lamellae in tweed orthoclase. Two narrow lamellae on the left are defect-free, but a thicker lamella on the right has two pairs of spike-like defects orientated parallel to a^*. Beam near to [001]. Fig. 9 (*right*). Bright-field TEM image of an albite lamella which is locally Albite-twinned. Beam near to [001].

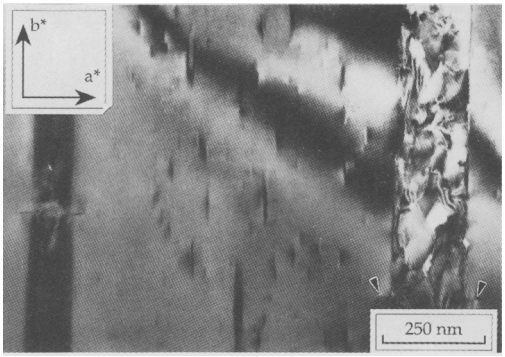

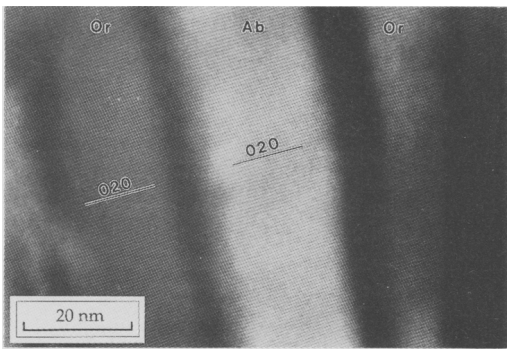

FIG. 10 and 11. Fig. 10 (*left*). Bright-field TEM image of a complex area of feldspar. On the left of the image is an apparently untwinned albite lamella with a prominent pair of defects. On the right side is a former albite lamella which has been completely replaced by a mosaic of interlocking K-feldspar subgrains, but has retained the defects (arrowed). In between the two lamellae is tweed orthoclase which contains numerous defect-free albite platelets. Beam near to [001]. Fig. 11 (*right*). TEM lattice image of an albite platelet (Ab) in tweed orthoclase (Or). (020) lattice fringes can be traced uninterrupted across the interface between albite and orthoclase. Beam parallel to [102].

SAED patterns of platelet-rich areas show a strong streaking parallel to a^* between orthoclase reflections and weak single albite spots from the untwinned platelets. This exaggerated streaking is a result of the fine size and morphology of the platelets, as was also described by Brown and Parsons (1988*a*) for sanidine platelets in a crypto-antiperthite. Lattice images of Shap platelets show that (020) fringes can be traced uninterrupted from albite to orthoclase along boundaries at least 70 nm in length (Fig. 11). This is interpreted to show that the platelets are fully coherent. Because albite and orthoclase have similar cell parameters and X-ray work shows that in perthites the two lattices are usually strained, which means that their cell parameters are even closer, we consider that it is reasonable to assume that in a [001] lattice image, (020) fringes for albite and orthoclase at a given defocus would be continuous across a coherent interface. Furthermore, as Brown and Parsons (1984) have demonstrated, defects such as dislocations rapidly damage under the electron beam in the TEM. No such areas of beam damage are evident in Fig. 11, further supporting the assertion that this interface is fully coherent.

Straddling film lamellae are pairs of defects ~50 nm in length which are very susceptible to electron beam damage. These defects lie within tweed orthoclase and in [001] images are aligned parallel to (020) of orthoclase (Figs. 8 and 10). In some cases, the defects appear to continue through film lamellae where they are again parallel to (020) of albite. The defects occur along both Albite-twinned and untwinned parts of film lamellae and die out as the films narrow towards their wedge-shaped ends. The separation of these defects is comparable to the spacing of etch pits along narrow HF acid-etched lamellae (Fig. 5)

Alteration microtextures. Two forms of lamella-specific alteration were imaged by TEM, both of which are exclusive to film lamellae. One form is characterised by numerous angular micropores ~30–200 nm in size, in between which the original albite has been replaced by a mosaic of irregular microcline subgrains (Fig. 10). These are comparable to the micropore-rich lamellae seen in BSE and SE images. However, there is a complete gradation from pristine lamellae containing an isolated micropore (Fig. 9) to complete replacement (Fig. 10). In the thickened lamellae, original albite has largely escaped alteration but it is encrusted by numerous outgrowths of Albite-twinned albite (as seen with SEM, Figs. 2 and 7). The regularly-spaced defects characteristic of film lamellae still occur along both forms of altered lamellae.

Veins and patch perthites cross-cut tweed orthoclase, albite films and occasionally also platelets (Fig. 12). They comprise micropore-rich intergrowths of irregular microcline (as defined by Bambauer *et al.*, 1989) with some Albite-twinned albite. In one case, we observed what appears to be Albite-twinned tweed orthoclase (Fig. 13). Albite subgrains have been imaged much less often than irregular microcline, but this may be an artefact of foil preparation, with areas of irregular microcline within orthoclase (all K-feldspar) thinning much more uniformly than large albite crystals enclosed by orthoclase. The interface between albite and orthoclase in patch perthites is sharp, commonly

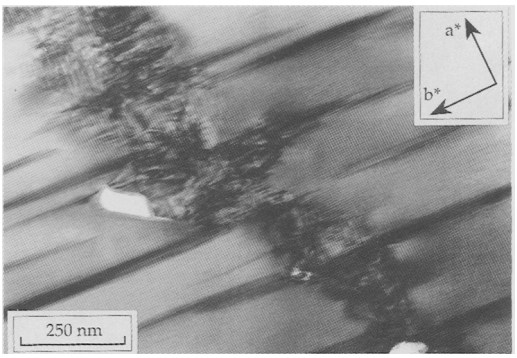

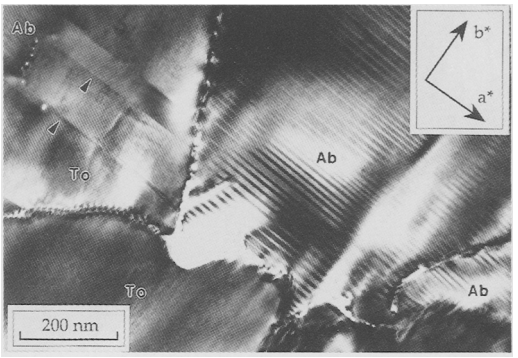

FIGS. 12 and 13. Fig. 12 (*left*). Bright-field TEM image of an area of pristine albite lamellae in tweed orthoclase which has been cross-cut by a vein of irregular microcline. The irregular microcline is associated with a number of micropores. Beam near to [001]. Fig. 13 (*right*). Bright-field TEM image of an area of coarsening in which a number of crystals of albite (Ab) and tweed orthoclase (To) can be seen. Numerous defects occur along the boundary of the large Albite-twinned albite crystal in the centre of the field of view. These defects are sites of selective electron beam damage. One crystal of tweed orthoclase appears to contain Albite twins (arrowed). Beam near to [001].

incoherent, and delineated by numerous defects (Fig. 13). However, the boundary between irregular microcline and tweed orthoclase is much more diffuse and lattice fringe images show that the interface can be coherent on a nm scale. Very few dislocations have been imaged at the interface (Figs. 12 and 14).

Micropores within patch perthites range from anhedral to euhedral in shape, the euhedral ones defining negative crystals with {110} terminations (Figs. 12 and 15). In one case, a micropore within irregular microcline contained phyllosilicate crystals with a ~1.4 nm lattice fringe spacing, possibly a chlorite. Irregular microcline is characterised by discontinuous Albite twins with uneven composition planes and has few Pericline twins (Figs. 12, 14 and 15). Low order reflections in SAED patterns have rows of two or three Albite twin reflections, representing fine-scale intergrowths of twinned and untwinned K-feldspar. In addition to twins, images of irregular microcline also show a diffuse tweed-like modulation which is oriented normal to the Albite twins and extends through them (Figs. 14 and 15). Importantly, in some cases where a vein of irregular

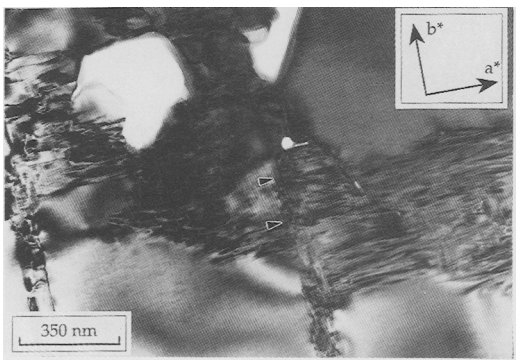

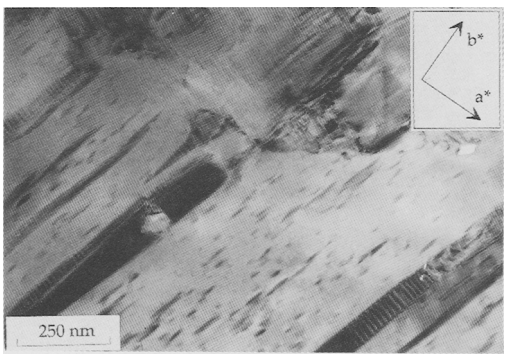

FIGS. 14 and 15. Fig. 14 (*left*). Bright-field TEM image of a vein of irregular microcline which cross-cuts albite lamellae and tweed orthoclase. The irregular microcline contains a number of micropores, but within it 'ghosts' of preexisting albite lamellae can also be seen (arrowed). Beam near to [001]. Fig. 15 (*right*). Bright-field TEM image showing an area of film lamellae and platelets which is cross-cut by an area of irregular microcline (top centre). Most of the film lamellae are both Albite-twinned and apparently untwinned. Beam near to [001].

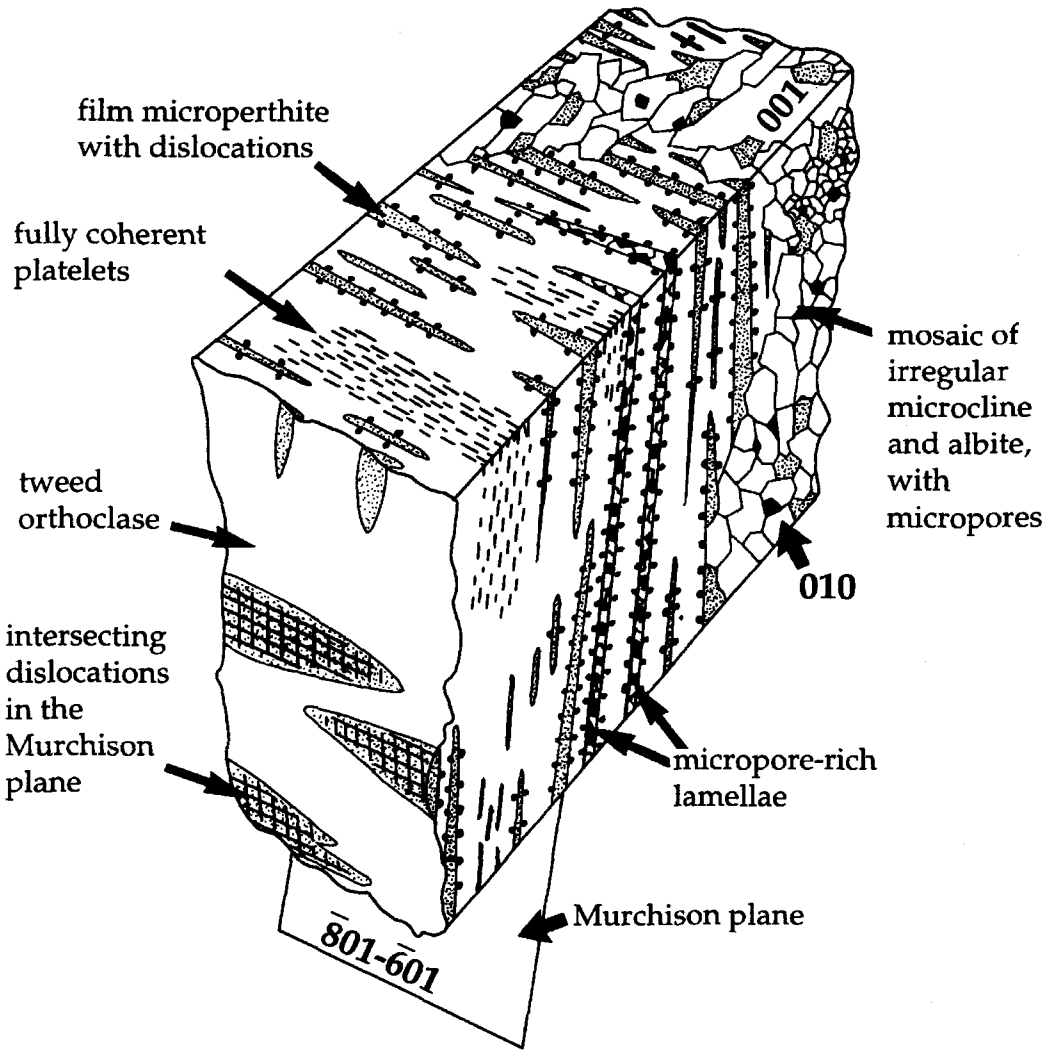

FIG. 16. Generalised sketch of a typical cleavage fragment of a Shap phenocryst. Albite is shown with a fine stipple, micropores as angular black areas and dislocations as small black circles. The different elements are not drawn accurately to scale but the length of the fragment would typically be about 0.1 mm. About 25% of the phenocryst is a deuterically altered band comprising albite and irregular microcline (far end); the remainder is predominantly pristine, fully coherent or sub-regularly semicoherent crypto- and microperthitic tweed orthoclase. Occasional micropore-rich altered lamellae occur within the otherwise pristine perthite.

microcline cross cuts albite lamellae, 'ghosts' of the lamellae can be seen within irregular microcline (Fig. 14). The cross-cutting character of the deuteric recrystallization is clearly seen in Fig. 15. The boundary between tweed orthoclase with platelets and irregular microcline is sharp and clearly cuts both the film cryptoperthite lamellae and platelets.

Discussion

Pristine microtextures

Nucleation of exsolution lamellae. The size of albite exsolution lamellae in Shap alkali feldspars is extremely variable on a 100s of nm scale. This

apparent irregularity is in part the result of the three dimensional morphology of film lamellae, which is comparable to that of an aeroplane wing (Fig. 16). Thus, the size of any one lamella imaged on a (001) cleavage surface will be a function of where that cleavage plane intersects the lamella in relationship to its three dimensional structure (i.e. a section across the middle of the wing will show its maximum cross-sectional length and width, whereas a section close to the tip of the wing will produce an apparently much shorter and narrower lamella). This cut effect, however, would be expected to produce lamellae of a fairly random size distribution and cannot account for the distinct differences in sizes between films and platelets.

In minerals, exsolution lamellae with bimodal size distributions have previously been described from pyroxenes by Champness and Lorimer (1976), amphiboles by Gittos *et al.* (1976) and feldspars by Brown and Parsons (1983) and Evangelakakis *et al.* (1993). Brown and Parsons (1983) described 5–25 nm oligoclase platelets between coarser oligoclase exsolution lamellae in a cryptoperthite from the Klokken syenite. They inferred that the coarse lamellae formed by heterogeneous nucleation on a perthite–perthite boundary, whereas platelets grew at lower temperatures by homogeneous nucleation. Evangelakakis *et al.* (1993) proposed a similar model for the origin of different-sized albite exsolution lamellae in Or-rich perthites from granulite grade metamorphic rocks. They suggested that coarse albite films grew from grain boundaries by heterogeneous nucleation, whereas finer spindles in grain interiors formed at lower temperatures by homogeneous nucleation. Comparisons with these studies suggests that the main episode of exsolution in Shap alkali feldspars was by heterogeneous nucleation, which produced the coarse film lamellae. Platelets grew at lower temperatures by homogeneous nucleation.

Dislocation periodicities. Defects that decorate the margins of albite lamellae in TEM images correspond closely in position and spacing to the etch pits imaged on HF etched samples (Fig. 5). The ends of the defects are interpreted to be the sites of edge dislocations. Owing to the high strain around these dislocations, they beam damage very rapidly and are also sites of preferential chemical etching, producing pits. Each albite lamella has two sets of dislocations oriented nearly at 90° to each other which form a network over its surface, as shown by images of the Murchison plane (Figs. 6 and 16). The defects imaged on (001) cleavage surfaces and [001] TEM foils are interpreted to be (020) misfit dislocations and those on (010) cleavage surfaces, (001) misfit dislocations. The pairs of dislocations seen on planar sections are the outcrops of single dislocation loops forming long, flat ellipses around the exsolution lamellae. Platelets, which are < 75 nm in width, can accommodate lattice mismatch by elastic strain and so are able to remain coherent.

Few examples of periodic dislocations have previously been reported in strain-controlled perthites (Smith and Brown, 1988). However, Brown and Parsons (1984) predicted that periodic dislocations should be common in Or-rich feldspars (> Or_{75}) from slowly-cooled rocks in which the migration of perthite interfaces into minimum strain orientations ($\bar{6}\bar{6}1$) has been blocked. Indeed, periodic dislocations have been observed in Or-rich microperthites using etching techniques (Aberdam, 1965; Wilson and McHardy, 1980) and TEM (Gandais *et al.*, 1974; Willaime *et al.*, 1976). Aberdam (1965) described etch pits straddling HF-etched albite lamellae, which he interpreted to represent the sites of dislocations. The spacing of these dislocations correlated well with lamella width (Aberdam, 1965). After subjecting a microcline perthite to hydrothermal etching, Wilson and McHardy (1980) also noted etch pits straddling albite exsolution lamellae which they again interpreted to represent the sites of dislocations. The dislocations described by Gandais *et al.* (1974) were edge dislocations in a microperthite ($Or_{72}Ab_{26}An_2$) and had periodicities of between 150 and 400 nm, depending on the local thickness of albite lenses. Willaime *et al.* (1976) recorded similar periodicities of 200–1000 nm for microperthite lamellae.

Dislocations form in strain-controlled microperthites as a result of the difference in cell dimensions between orthoclase and albite. From standard X-ray data, the (020) lattice planes of low albite (~0.638 nm) have 98.5% of the spacing of the (020) planes of orthoclase (~0.648 nm). Using the technique of Aberdam (1965), this difference in spacing means that in order to minimise strain energy, and assuming there is no homogeneous strain in either phase, one dislocation should occur in orthoclase every 41.3 nm along the albite–orthoclase interface, but this is clearly not the case (Fig. 5). To produce the observed dislocation spacings of 250–700 nm, the difference on (020) lattice spacings between orthoclase and albite would have to be ~0.1 to 0.3%. Assuming that dislocations imaged on (010) cleavage surfaces are (001) misfit dislocations, a comparable ideal spacing of 44.5 nm can be calculated from standard X-ray data. These discrepancies are in contrast to dislocation spacings calculated for a ternary mesoperthite from the Klokken syenite which agree very well with observed spacings of 100–150 nm (Brown and Parsons, 1984).

Part of the discrepancy between calculated and observed dislocation spacings could be because some

dislocations do not etch out during HF treatment, but as Fig. 5 shows, there is little difference between dislocation spacings determined from the etched cleavage surfaces and TEM foils. Stress can be taken up by homogeneous and heterogeneous elastic strain, as shown by the smallest films and platelets which have remained coherent. For the extended lamellae, strain between orthoclase and albite has been only partially accommodated by periodic dislocations, and it is most probable (as the defect spacings calculated above suggest) that there is residual homogeneous strain in both phases but predominantly in the subordinate albite. Strain is also reduced by periodic Albite twinning in the albite. As the crystals cooled, two factors, lamellar coarsening and the increasing stiffness of the structure, would have governed the spontaneous appearance of dislocations. Strain would have been defined locally by the proximity of clusters of lamellae and their size distribution, and strain would vary from point to point in the structure. This accounts for the large scatter in the relationship between lamellar thickness and dislocation spacing (Fig. 5) and implies that the dislocations formed over a range of temperatures and most probably at relatively low temperature when the structure was stiff. The better agreement between differences in cell parameters and dislocation spacing found by Brown and Parsons (1984) for a crypto- mesoperthite and their much greater regularity in spacing are consistent with formation at much higher temperatures (as expected from solvus relationships) when the structure was comparatively less stiff.

Twinning in albite. The apparently untwinned parts of albite lamellae in Shap are interpreted to be Pericline-twinned, because such twins cannot be imaged in Na-plagioclase when looking down [001]. Although quantitative information was not collected during this study, Pericline twinning appears to be at least as common as Albite twinning in Shap exsolution lamellae. Albite and Pericline twins develop in the albite to minimise coherency strain energy by the development of corrugations along the albite–orthoclase interface. These corrugations lie close to minimum strain orientations which are approximately ($\bar{6}31$) and ($\bar{3}31$) (Willaime and Brown, 1974; Fleet, 1982). The tweed microstructure, which comprises a very fine scale coherent intergrowth of nm-sized ordered–antiordered domains, forms during the monoclinic–triclinic transformation in K-feldspar. It, too, has significant strain energy (Brown and Parsons, 1993).

Temperature evolution of pristine microtextures

The temperature evolution of the microtextures can be estimated approximately from phase equilibrium considerations. Shap is a two-feldspar, subsolvus granite, and it would have crystallized a plagioclase and a homogeneous alkali feldspar (probably low sanidine) in equilibrium on the strain-free ternary feldspar solvus. In principle, if complete stable equilibrium were maintained during subsequent cooling, reciprocal intercrystal exchange of the three components, Ab, An and Or, would occur and both plagioclase and alkali feldspar would follow paths on the ternary strain-free solvus leading ultimately to a rock containing two homogeneous feldspar phases. In practice (and in common with most, perhaps all, feldspar pairs in igneous rocks), the feldspars did not maintain intercrystal exchange equilibrium but left the strain free solvus. The alkali feldspar intersected the coherent solvus leading to the strain-controlled microperthites. The extent of intercrystal exchange equilibrium prior to exsolution is not easy to establish; most applications of two-feldspar geothermometry to granitic rocks assume that the crystals maintain their magmatic bulk compositions down to low T, although there is evidence of intercrystal exchange in granulites (Brown and Parsons 1988*b*; Evangelakakis *et al.* 1993). However, the bulk composition of the pristine crystals ($Or_{75.1}Ab_{24.5}An_{0.4}$) can be used to estimate a *minimum* crystallization temperature using its relationship to the strain-free solvus, and a *maximum* temperature for the beginning of coherent exsolution may be obtained from the coherent solvus. These curves were reviewed by Brown and Parsons (1989). Complications are introduced by Si,Al ordering and by the small An-content of the alkali feldspar which has an extremely large effect on exsolution temperatures.

If the effect of anorthite is ignored, temperatures may be estimated from Fig. 8 in Brown and Parsons (1989). Assuming P of 0.1 GPa, these solvi, which take account of Si,Al ordering, suggest that the crystals grew at *at least* $\geqslant$580°C, and began to exsolve at or below $\leqslant$460°C. This is 110°C above the equivalent T for disordered feldspars (Smith and Parsons, 1974). In addition, the ternary solvus is extremely steep along lines of constant Ab:Or, but experimentally poorly constrained. For ordered feldspars there are no experimental data, but an estimate of the effect of An can be made using a variety of two-feldspar geothermometers which are based on experimental data (largely unreversed) for disordered feldspars at higher T. Using the program SOLVCALC (provided by H. Nekvasil and S. Wen; SUNY, Stony Brook) we searched for thermometers that gave a reasonable agreement with the reversed binary Ab–Or solvus of Smith and Parsons (1974). The thermometers of Elkins and Grove (1990) and Fuhrman and Lindsley (1988) fulfil this criterion to within ~20°C. Both thermometers suggest that, if disordered, the Shap alkali feldspars crystallized at or

above 600°C. In other words, 0.4 mol% An increases exsolution T in the Shap alkali feldspars by ~130°C. Adding 110°C to take account of ordering would suggest crystallization at a minimum of about 710°C, and commencement of coherent exsolution at 590°C, if we assume that the ternary coherent solvus for ordered frameworks is at T ~120°C lower than the strain-free ternary solvus, the difference for binary solid solutions. It is, however, probable that the alkali feldspar grew initially with a higher degree of disorder than the equilibrium degree of order at these T, and therefore 710°C for the minimum growth T is likely to be an overestimate. Caunt (1986) provided analyses of coexisting plagioclases ranging from $An_{25}Ab_{70}Or_5$ to $An_6Ab_{89}Or_5$. Using the Fuhrman and Lindsley (1988) two-feldspar thermometer gives 675°C for the An_{25} plagioclase, but $T <$ 550°C using the An_6 plagioclase. This suggests that the alkali feldspar crystallized in equilibrium with the more basic plagioclase, but the estimates again assume that both feldspars were disordered at the time equilibrium was reached. However, taking all these factors into account, it seems reasonable to conclude that the alkali feldspars grew at ~700°C, and that coherent exsolution began at ~590°C.

At first, when the exsolution lamellae were small, they would have been fully coherent and strain would have been homogeneous or accommodated by the wedge-shaped terminations of the lamellae. However, as they coarsened and the feldspar structure became stiffer, dislocations would have to form to accommodate the misfit at the interface. As we argued in the preceding section, it is probable that this would occur over range of temperatures, depending on the local evolution of the exsolution lamellae. Finally, also at lower temperature, Na–K interdiffusion became slow and coherent platelets began to form by homogeneous nucleation. An absolute maximum T for platelet formation can be obtained from the bulk composition of areas with platelets. The proportion of matrix orthoclase and platelets in Figs 3, 10 and 15 suggests a bulk composition of ~Or_{90} (assuming that exsolution has gone to completion). This implies exsolution of the platelets at < 400°C. It is possible that this represents a sustained period at some lower temperature, but this is not necessary to the development of two-stage exsolution textures.

The potassium feldspar in volumes of the crystal unaffected by deuteric alteration is tweed orthoclase. This represents a stage in textural evolution reached by ~500°C (Brown and Parsons, 1989); at this point the tweed texture became stranded and the feldspar did not order further as it entered the field of intermediate and, ultimately, low microcline at < 450°C. The platelets therefore formed in a matrix of tweed orthoclase. Elsewhere, the crystals were affected by deuteric alteration and experienced a different low-T textural history; this is described in the following section.

Turbid microtextures

Origin of micropores. Turbidity is a common feature of alkali feldspars, caused by light scattering by μm-scale micropores which may be fluid-filled (Worden *et al.*, 1990; Walker, 1991; Burgess *et al.*, 1992). The formation of micropores has previously been shown to be associated, in hypersolvus igneous rocks, with large-scale textural and chemical reorganization during which crypto- and microperthites coarsen by a factor of ~10^3 into coarse, largely incoherent, patch perthite intergrowths (Parsons, 1978; Worden *et al.*, 1990; Guthrie and Veblen, 1991). Turbidity in the Shap alkali feldspars is similarly closely associated with textural alteration and coarsening of perthite; 10–30% of each feldspar is affected. Walker (1991) measured the microporosities of pink alkali feldspars from a number of different intrusions (including the Shap granite) and found a range from 0.5 to 2.5 vol%. In only one case during the present study was a non-feldspar phase found within a micropore (an ~1.4 nm phyllosilicate). However, Walker (1991) analysed particles within micropores in Shap alkali feldspars by analytical SEM and found non-feldspar elements including Mg, Cl, Fe, Mn and Ti. The fluid which altered the Shap granite feldspars was probably mainly deuteric in origin, but a component of the hydrothermal brines which produced the small-scale epigenetic mineralization within the granite cannot be discounted. Firman (1978) suggested that the red colour of alkali feldspar phenocrysts was caused by iron released during alteration of biotite.

Dissolution and reprecipitation of feldspar. Alteration has had a profound affect on the microtexture of the Shap phenocrysts and two main styles of alteration have been recognised: (i) selectively altered albite lamellae and (ii) cross-cutting veins and patch perthites (Fig. 16). During selective alteration there has either been a net loss of albite, producing micropore-rich lamellae and lamellae altered to irregular microcline, or a net gain of albite, resulting in thickened lamellae. The selectivity of alteration of coarse film lamellae indicates a strong microtextural control on the movement of fluids through Shap feldspars. This is exemplified by the occurrence of altered lamellae in discrete groups which are interpreted to represent areas of preferential fluid movement and interaction. The reason why film lamellae have exerted such a strong influence on fluid movement is probably a result of their size and semi-coherency. The selectivity suggests that lamellae, and the dislocations, commonly

reach crystal surfaces or major fractures. In contrast, the fully coherent exsolution lamellae in cryptoperthites and in alkali feldspars from the Klokken syenite appear to have exercised no control on fluid penetration into the crystals (Worden *et al.* 1990). As demonstrated by Walker (1990), networks of micropores are permeable. Once pores have formed in the albite lamellae, fluids can advance rapidly through them, and new feldspar can form by replacement laterally in adjacent feldspar (Fig. 7). The deuteric reactions clearly occurred at a lower T than the coherent exsolution, coherent coarsening, formation of dislocations, and formation of platelets, i.e. $\leqslant 400°C$. For more Or-rich feldspars than those from Shap, $T < 300°C$ are implied, and several lines of evidence suggest that recrystallization may continue to near-surface T (Brown and Parsons, 1993).

Cross-cutting veins of irregular microcline and the larger scale patch perthites have resulted from alteration of both albite lamellae and tweed orthoclase. The formation of micropores shows that alteration is not a constant volume replacement reaction; the volume of albite and irregular microcline which has been reprecipitated is smaller that the volume of tweed orthoclase and albite removed by dissolution. The sink for excess albite and microcline in the Shap granite is not known. In some cases, the micropores are concentrated along the margins of the altered areas and present negative crystal faces to the surrounding tweed orthoclase (Fig. 7). Irregular microcline crystals which terminate in these pores have euhedral terminations. In these cases, it would appear that there was an intermediate stage of open porosity between dissolution of tweed orthoclase and reprecipitation of irregular microcline. However, in other examples, 'ghosts' of former albite lamellae can be seen within areas of irregular microcline (Fig. 14) indicating that the transformation in this cases was on a very fine (nm) scale, with little or no intermediate porosity.

The process of transformation of tweed orthoclase to microcline has been termed 'unzipping' by Brown and Parsons (1989). The thermodynamic driving forces for this reaction are the release of elastic strain energy of the tweed microstructure and a small increase in Si,Al order of the newly formed microcline (both of which lead to a decrease in Gibbs free energy). The total energy released by unzipping of tweed orthoclase to low microcline is $\sim 2-3$ kJmol^{-1} (Brown and Parsons, 1993). Waldron *et al.* (1993) suggested that the unzipping of tweed orthoclase is an intracrystalline dissolution–reprecipitation reaction. However, tweed-like modulations persist within Shap irregular microcline and comparable microstructures were recorded by Fitz Gerald and Harrison (1993). An intermediate stage in the unzipping of tweed orthoclase to irregular microcline may be represented by the apparently Albite-twinned tweed orthoclase imaged in a patch perthite (Fig. 13). We have not been able to investigate this isolated feature further, but it is perhaps a result of minor stress exerted from outside the tweed area, and hence the features are strictly pseudotwins (Brown and Macaudière, 1986). Alternatively the texture could result from imbalance in ordered and antiordered domains in adjacent 'twins' although it is not obvious how such a situation could arise.

Although the alteration of the Shap feldspars was driven by minimisation of coherent elastic strain and interface energy, microtextures also controlled the ability of fluids to penetrate the crystals and facilitate the unzipping process. Cryptoperthite patches, which are fully coherent and have a large number of interfaces per unit area, have been altered very little. In principle, these cryptoperthites should be more susceptible to alteration than the microperthites in which the dislocations have decreased much, although not all, of the interfacial strain energy. The penetration of water along the dislocations was the controlling factor, not the total strain. The observation that alteration varies greatly in extent within any one area of a crystal implies that pathways of rapid fluid advection, such as open fractures, must have controlled the movement of deuteric fluids through the crystals on a large (μm) scale.

There is a strong selectivity for alteration to albite lamellae, leaving the tweed orthoclase, with which the lamellae are in intimate contact, often completely unaltered. This implies that in these particular deuteric fluids, albite was more susceptible to dissolution than orthoclase. This is exemplified by near-total removal of albite from some areas of alteration and reprecipitation of irregular microcline in its place. The remobilized albite was later reprecipitated in large albite-rich areas of patch perthites. The temporal and spatial relationships between those fluids which were dissolving albite/orthoclase and those which were reprecipitating albite/irregular microcline is difficult to determine. There may have been several discrete events of dissolution and of reprecipitation in response to fluctuations in fluid chemistry and external temperature and pressure conditions. Within any one feldspar crystal, there must be extensive fluid transport of Na and K. If these cations manage to leave their parent feldspar crystal, they must do so in near-equal proportions because the bulk compositions of turbid and pristine feldspar are similar.

Conclusions

The anatomy of a Shap alkali feldspar phenocryst is summarized in Fig. 16. Each crystal has a 'dual

microtexture', a feature found in the Klokken and Coldwell syenites (Worden *et al.*, 1990; Waldron and Parsons, 1992), the Skye epigranites (Guthrie and Veblen, 1991; Burgess *et al.*, 1992) and the Chain of Ponds pluton (Fitz Gerald and Harrison, 1993). We are familiar with similar textural variety in feldspars from a large number of granites from Scotland and elsewhere (Walker, 1991). Parts of each Shap phenocryst contain pristine microstructures, in which perthite lamellae are either all coherent or, some fully coherent and some subregularly semi-coherent. The remainder of each crystal is deuterically altered to a much more irregular, microporous and micropermeable patch perthite (Fig. 16). The pristine feldspar has been pervasively replaced by a mosaic of albite and K-feldspar subgrains as a result of a dissolution-reprecipitation process. The transition of tweed orthoclase to irregular microcline was also promoted during the deuteric reactions. The amount of deuteric alteration is likely to vary somewhat between different examples of phenocryst, and it is the feature which is largely responsible for the colour, translucency and subsequent chemical reactivity of the feldspar. The driving force for the deuteric reactions is reduction of elastic strain energy in crypto- and micro-perthite lamellae, and in the tweed domain texture of orthoclase.

The textures are of great importance in the argon systematics of alkali feldspars (Parsons *et al.*, 1988; Burgess *et al.*, 1992; Fitz Gerald and Harrison, 1993). In the case of the Shap feldspars the penetration of fluids deep into the crystals was facilitated by dislocations at the interface of the thicker exsolution lamellae, and this suggests that these dislocations would also act as pathways for the relatively rapid loss of radiogenic argon. Regions with fine-scale coherent cryptoperthite would be retentive. Regions with deuteric textures would undoubtedly have their argon isotopic system reset at the time of the fluid-feldspar interactions, and the resulting mosaic provides an effective trap for loosely retained argon in fluid inclusions and dislocations. The retentivity of K-feldspar subgrains in these regions would be highly variable, depending on their size and the availability of escape routes for argon to the crystal surface.

The textural evolution of the Shap alkali feldspars can be summarized as follows:

1. The first exsolution lamellae to form were coarse albite films which grew by heterogeneous nucleation beginning at 590°C. Later, and at lower temperatures, coherent platelets < 75 nm in thickness grew between the films by homogeneous nucleation which continued to below 400°C.

2. Spaced dislocations developed at the edges of thicker lamellae as the structure stiffened with decreasing temperature. The temperature at which the dislocations formed and the spacing between them depended on the thickness of lamellae and the local strain.

3. Deuteric alteration at $T < 400$°C resulted in dissolution of coherent or semi-coherent albite and tweed orthoclase and reprecipitation of incoherent to semi-coherent intergrowths of irregular microcline and albite.

4. The movement of deuteric fluids through Shap feldspars was partially controlled by the distribution of the coarse, subregular semi-coherent albite film lamellae which allowed fluid ingress into the interior of the phenocrysts. Most tweed orthoclase, and albite in platelets, which are fully coherent, remains unaltered. Altered volumes are microporous and micropermeable. The weathering of such feldspars will be strongly dependent on the presence of dislocations.

5. The main driving force for deuteric alteration is inferred to have been a decrease in the elastic strain energy at the coherent interfaces of crypto- and micro-perthite lamellae, and the recrystallization of tweed orthoclase, with strain in domain walls, to irregular microcline.

Acknowledgements

We would like to thank Mike Hall for making the thin sections and Chris Jeffree and David Hulmes for provision of SEM and TEM facilities respectively. This paper benefited considerably from discussions with Bill Brown and comments from two anonymous referees. This study was funded by NERC research grants GR3/6695 and GR3/8374.

References

Aberdam, D. (1965) Utilisation de la microscopie electronique pour l'etude des feldspaths. Observations sur des microperthites. *Sci. de la Terre*, **6**, 76 pp.

Aveline, W. T., Hughes, T. McK. and Strahan, A. (1888) *The geology of the country around Kendal, Sedbergh, Bowness and Tebay*. Mem. Geol. Surv. U. K., 94 pp.

Bambauer, H. U., Krause, C. and Kroll, H. (1989) TEM-investigation of the sanidine/microcline transition across metamorphic zones. *Eur. J. Mineral.*, **1**, 47–58.

Bott, M. H. P. (1974) The geological interpretation of a gravity survey of the English Lake District and the Vale of Eden. *J. Geol. Soc. London*, **130**, 309–31.

Brown, W. L. and Macaudière, J. (1986) Mechanical twinning of plagioclase in a deformed meta-anorthosite. *Contrib. Mineral. Petrol.*, **92**, 44–56.

Brown, W. L. and Parsons, I. (1983) Nucleation on

perthite-perthite boundaries and exsolution mechanisms in alkali feldspars. *Phys. Chem. Minerals*, **10**, 55–61.

Brown, W. L. and Parsons, I. (1984) The nature of potassium feldspar, exsolution microtextures and development of dislocations as a function of composition in perthitic alkali feldspars. *Contrib. Mineral. Petrol.*, **86**, 335–41.

Brown, W. L. and Parsons, I. (1988*a*) Zoned ternary feldspars in the Klokken intrusion: exsolution microtextures and mechanisms. *Contrib. Mineral. Petrol.*, **98**, 444–54.

Brown, W. L. and Parsons, I. (1988*b*) Intra- and intergrain exchange and geothermometry in granulite-facies feldspars. *Terra Cognita*, **8**, 263.

Brown, W. L. and Parsons, I. (1989) Alkali feldspars: ordering rates, phase transformations and behaviour diagrams for igneous rocks. *Mineral. Mag.*, **53**, 25–42.

Brown, W. L. and Parsons, I. (1993) Stored elastic strain energy: the driving force for low-temperature reactivity and alteration of alkali feldspar. In *Defects and Processes in the Solid State: Geoscience Applications. The McLaren Volume*, J. Boland and J. D. Fitz Gerald, (eds.), 267–90.

Burgess, R., Kelley, S. P., Parsons, I., Walker, F. D. L. and Worden, R. H. (1992). ^{40}Ar–^{39}Ar analysis of perthite microtextures and fluid inclusions in alkali feldspars from the Klokken syenite, South Greenland. *Earth Planet. Sci. Letters*, **109**, 147–67.

Caunt, S. L. (1986) *Igneous and metamorphic processes in the Shap granite and its aureole*. Unpubl. Ph.D. thesis, University of Leeds.

Champness, P. E. and Lorimer, G. W. (1976) Exsolution in silicates. In *Electron Microscopy in Mineralogy*, H. R. Wenk (ed.), 174–204.

Elkins, L. T. and Grove, T. L. (1990) Ternary feldspar experiments and thermodynamic models. *Amer. Mineral.*, 75, 544–59.

Evangelakakis, C., Kroll, H., Voll, G., Wenk, H-R., Meisheng, H. and Kopcke, J. (1993) Low-temperature coherent exsolution in alkali feldspars from high-grade metamorphic rocks of Sri Lanka. *Contrib. Mineral. Petrol.*, **114**, 519–32.

Firman, R. J. (1957) Fissure metasomatism in volcanic rocks adjacent to the Shap granite, Westmorland. *Q. J. Geol. Soc. London*, **113**, 205–22.

Firman, R. J. (1978) Intrusions. In *The Geology of the Lake District*, F. Moseley (ed.), 146–67.

Fitz Gerald, J. D. and Harrison, T. M. (1993) Argon diffusion in K-feldspar I: microstructures in MH-10. *Contrib. Mineral. Petrol.*, **113**, 367–80.

Fleet, M. E. (1982) Orientation of phase and domain boundaries in crystalline solids. *Amer. Mineral.*, **67**, 926–36.

Fuhrman, M. L. and Lindsley, D.H. (1988) Ternary-feldspar modelling and thermometry. *Amer. Mineral.*, **73**, 201–15.

Gandais M., Guillemin, C. and Willaime, C. (1974) Study of boundaries in cryptoperthites. *Eighth Int. Cong. Elec. Micros. Canberra*, 508–9.

Gittos, M. F., Lorimer, G. W. and Champness, P. E. (1976) The phase distributions in some exsolved amphiboles. In *Electron Microscopy in Mineralogy*, H. R. Wenk (ed.), 238–47.

Grantham, D. R. (1928) The petrology of the Shap granite. *Proc. Geol. Ass.*, **39**, 299–331.

Guthrie, G. D. and Veblen, D. R. (1991) Turbid alkali feldspars from the Isle of Skye, northwest Scotland. *Contrib. Mineral. Petrol.*, **108**, 298–304.

Harker, A. and Marr, J. E. (1891) The Shap granite and associated igneous and metamorphic rocks. *Q. J. Geol. Soc. London*, **47**, 266–327.

Harker, A. and Marr, J. E. (1893) Supplementary notes on the metamorphic rocks around the Shap granite. *Q. J. Geol. Soc. London*, **49**, 359–71.

Lee, M. K. (1986) A new gravity survey of the Lake District and three-dimensional model of the granite batholith. *J. Geol. Soc. London*, **143**, 425–35.

Locke, C. A. and Brown, G. C. (1978) Geophysical constraints on structure and emplacement of Shap granite. *Nature*, **272**, 526–8.

Nicholson, H. A. (1868) On the granite of Shap in Westmorland. *Trans. Edinb. Geol. Soc.*, **1**, 133–7.

Parsons, I. (1978) Feldspars and fluids in cooling plutons. *Mineral. Mag.*, **42**, 1–17.

Parsons, I., Rex, D. C., Guise, P. and Halliday, A. N. (1988) Argon-loss by alkali feldspars. *Geochim. Cosmochim. Acta*, **52**, 1097–112.

Smith, J. V. and Brown, W. L. (1988) *Feldspar minerals. Vol. 1, Crystal structures, chemical and microtextural properties*. 2nd edition. Springer-Verlag, Berlin.

Smith, P. and Parsons, I. (1974) The alkali feldspar solvus at 1 kilobar water vapour pressure. *Mineral. Mag.*, **39**, 747–67

Soper, N. J. and Kneller, B. C. (1990) Cleaved microgranite dykes of the Shap swarm in the Silurian of NW England. *Geol. J.*, **25**, 161–70.

Wadge, A. J., Gale, N. H., Beckinsale, R. D. and Rundle, C. C. (1978) A Rb–Sr isochron for the Shap granite. *Proc. Yorks. Geol. Soc.*, **42**, 297–305.

Waldron, K. and Parsons, I. (1992) Feldspar microtextures and multistage thermal history of syenites from the Coldwell Complex, Ontario. *Contrib. Mineral. Petrol.*, **111**, 222–34

Waldron, K., Parsons, I. and Brown, W. L. (1993) Solution-redeposition and the orthoclase-microcline transformation: evidence from granulites and relevance to ^{18}O exchange. *Mineral. Mag.*, **57**, 687–95.

Waldron, K., Lee, M. R. and Parsons, I. (1994) The microstructures of perthitic alkali feldspars revealed by hydrofluoric acid etching. *Contrib. Mineral.*

Petrol., **116**, 360–4.

Walker, F. D. L. (1990) Ion microprobe study of intragrain micropermeability in alkali feldspar. *Contrib. Mineral. Petrol.*, **106**, 124–8.

Walker, F. D. L. (1991) *Micropores in alkali feldspars.* Unpubl. Ph.D. thesis. University of Edinburgh.

Willaime, C. and Brown, W. L. (1974) A coherent elastic model for the determination of the orientation of exsolution boundaries: application to feldspars. *Acta Crystallogr.*, **A30**, 316–31.

Willaime, C., Brown, W. L. and Gandais, M. (1976) Physical aspects of exsolution in natural alkali feldspars. In *Electron Microscopy in Mineralogy*, H. R. Wenk, (ed.), 248–57.

Wilson, M. J. and McHardy, W. J. (1980) Experimental etching of a microcline perthite and implications regarding natural weathering. *J. Microsc.*, **120**, 291–302.

Worden, R., Walker, F. D. L., Parsons, I. and Brown, W. L. (1990) Development of microporosity, diffusion channels and deuteric coarsening in perthitic alkali feldspars. *Contrib. Mineral. Petrol.*, **104**, 507–14.

Zeitler, P. K. and Fitz Gerald, J. D. (1986) Saddle-shaped $^{40}Ar/^{39}Ar$ age spectra from young, microstructurally complex potassium feldspars. *Geochim. Cosmochim. Acta*, **50**, 1185–99.

[*Manuscript received 28 December 1993: revised 15 April 1994*]